Arab J Sci Eng (2016) 41:401–424
DOI 10.1007/s13369-015-1678-x

RESEARCH ARTICLE - CIVIL ENGINEERING

Behavior of RC Shallow and Deep Beams with Openings Via the Strut-and-Tie Model Method and Nonlinear Finite Element

Waleed E. El-Demerdash[1] · **Salah E. El-Metwally**[1] · **Mohamed E. El-Zoughiby**[1] · **Ahmed A. Ghaleb**[1]

Received: 22 January 2015 / Accepted: 23 April 2015 / Published online: 17 May 2015

Abstract The strut-and-tie model (STM) has been widely applied for the design of reinforced concrete (RC), members particularly discontinuity regions. In this paper, on the basis of available experimental results of crack patterns, failure modes, and trajectories of internal stresses from elastic finite element analysis (FEA), STMs have been suggested for many shallow and deep beams with openings, which had been tested experimentally. In addition, for comparison purposes, 3-D nonlinear FEA using ANSYS-12 package has been performed for selected beams. Some of the important factors affecting the behavior of RC beams, namely concrete compressive and tensile strength, span-to-depth ratio, shear span-to-depth ratio, physical and mechanical properties of horizontal, vertical web reinforcement and main steel, loading position, opening dimensions, and location, are investigated via a parametric study with the aid of 3-D nonlinear FEA. With such analysis, results of crack pattern, deflection, failure mode, and strain and stress distributions, which cannot be determined using the STM, are obtained. A comparison of the FEA with test results and proposed STMs has been carried out. The present study reveals the reliability of the STM method in obtaining a reasonable lower bound estimate of the load carrying capacity of RC ordinary/deep beams with openings. In addition, the 3-D nonlinear FEA of simple and continuous NSC and HSC ordinary/deep beams with/without openings yields accurate predictions of both the ultimate load and the complete response.

✉ Salah E. El-Metwally
selmetwally@yahoo.com

[1] Structural Engineering Department, Mansoura University, El-Mansoura, Egypt

Keywords Strut-and-tie model · 3-D nonlinear finite element analysis · Shallow and deep beams · Openings · Normal-strength concrete · High-strength concrete

1 Introduction

Inserting openings in the web of a reinforced concrete, RC, beam is associated with not only a sudden change in the dimensions of its cross section, but also a concentration of stresses at the corners of the opening, and it is possible to induce transverse cracks in the beam. Openings also reduce the stiffness, which leads to excessive deformations and considerable redistribution of forces.

In this paper, the behavior of selected RC shallow and deep beams with openings, constructed from normal-strength concrete, NSC, and high-strength concrete, HSC, is examined. Current codes, e.g., ACI 318M-11 [1], define a beam to be deep when the span-to-overall-depth ratio $L/h \leq 4$, or the shear span-to-overall-depth ratio $a/h \leq 2$. As a result of its proportions, the beam strength is usually controlled by shear, rather than by flexure, provided that normal amount of longitudinal reinforcement is used. Nevertheless, the shear strength of deep beams is significantly greater than that predicted using expressions developed for shallow beams.

The method of strut-and-tie model, STM, has proved to be a rational method for the analysis and design of discontinuity regions [2,3], D-regions; therefore, the method is utilized to carry out this investigation. In addition, the finite element package ANSYS-12 [4] is used to perform a 3-D nonlinear finite element analysis, FEA, of selected tested shallow and deep beams. The FEA, on one hand, is used to check the output results obtained from the STM and completes, on the other hand, the understanding of the behavior of the con-

sidered RC beams. The results of both STM and FEA are compared with the available test results.

2 The Approach to Develop a STM for a Beam with Openings

The approach for developing a STM for a beam with openings is illustrated in the following:

- Use equilibrium of the whole beam to find the external reactions.
- Follow the load path principle to construct the STM.
- The elements of a STM can be verified by performing a stress analysis using linear elastic FEA, which produces the stress trajectories. It is also possible to consider the nonlinear behavior and the cracking of concrete in the FEA. Generally, the strut and tie directions should be within $\pm 15^\circ$ of the direction of the compressive and tensile stress trajectories, respectively.
- External equilibrium of loads and reactions for the whole beam or the part around the opening and internal equilibrium at nodes have to be fulfilled.
- Diagonal struts are oriented parallel to and between the expected axis of cracking.
- Struts must not cross or overlap each other. Their widths are chosen to carry their forces using the effective strength of the concrete in the struts.
- Ties can cross struts or other ties. A STM with the least number of shortest ties is likely the best.
- Experimentally, the available crack patterns may assist in selecting the best STMs.
- The angle θ between the axis of a strut and a tie entering a single node shall be taken $\geq 25^\circ$.

3 Strength Limits of STM Components

For the proposed STMs, the strengths of ties, concrete struts, and nodal zones are as follows.

Reinforced Ties: In this paper, the contribution of tensile strength of a concrete tie is ignored and normally tie forces are carried by reinforcement. The tie cross section is constant along its length and is obtained from the tie force and the yield stress of steel. The *nominal strength* of a tie F_{nt} shall be taken as

$$F_{nt} = A_{st}\, f_y$$

where A_{st} and f_y are the cross-sectional area and yield stress of steel, respectively. Depending on the distribution of the tie reinforcement, the effective tie width w_t may vary between the following limits, with an upper limit given afterward.

Table 1 ACI 318M-11 Code [1] values of coefficient β_s of struts

Strut condition	β_s
A strut with constant cross section along its length	1.0
For struts located such that the width of the midsection of the strut is larger than the width at the nodes (bottle-shaped struts):	
(a) With reinforcement normal to the centerline of the strut to resist the transversal tensile force	0.75
(b) Without reinforcement normal to the centerline of the strut	0.60λ
For struts in tension members, or the tension flanges of members	0.40
For all other cases	0.60λ

$\lambda = 0.85$ for sand-lightweight concrete, 0.75 for all-lightweight concrete, and $\lambda = 1.0$ for normal-weight concrete

Table 2 ACI 318M-11 code [1] values of coefficient β_n of nodes

Nodal zone	β_n
Compression–compression–compression, C–C–C	1.00
Compression–compression–tension, C–C–T	0.80
Compression–tension–tension, C–T–T[a]	0.60
Tension–tension–tension, T–T–T	0.40

[a] In nodal zones anchoring two or more ties with the presence of one strut

- One row of bars without sufficient development length beyond the nodal zones:

$$w_t = 0.0$$

- One raw or more rows of bars and providing sufficient development length beyond the nodal zones for a distance not less than twice concrete cover $2c$:

$$w_t = n\emptyset_{bar} + 2c + (n-1)\, s$$

where $\emptyset_{bar}$ is the bar diameter, n is the number of bars, and s is the clear space between bars. The upper limit is established as the width corresponding to that in a hydrostatic nodal zone as:

$$w_{t,max} = F_{nt} / \left(f_{ce}^{n}\, b\right)$$

where b is the beam width and f_{ce}^{n} is the applicable effective compressive strength of a nodal zone and is computed from [1,5] as:

$$f_{ce}^{n} = 0.85 f_c' \beta_n \quad \text{or} \quad 0.67 f_{cu} \beta_n$$

The $0.85 f_c'$ stands for a cylinder concrete compressive strength, $0.67 f_{cu}$ for a cube concrete compressive strength, and β_n for the effectiveness factor of the nodal zone.

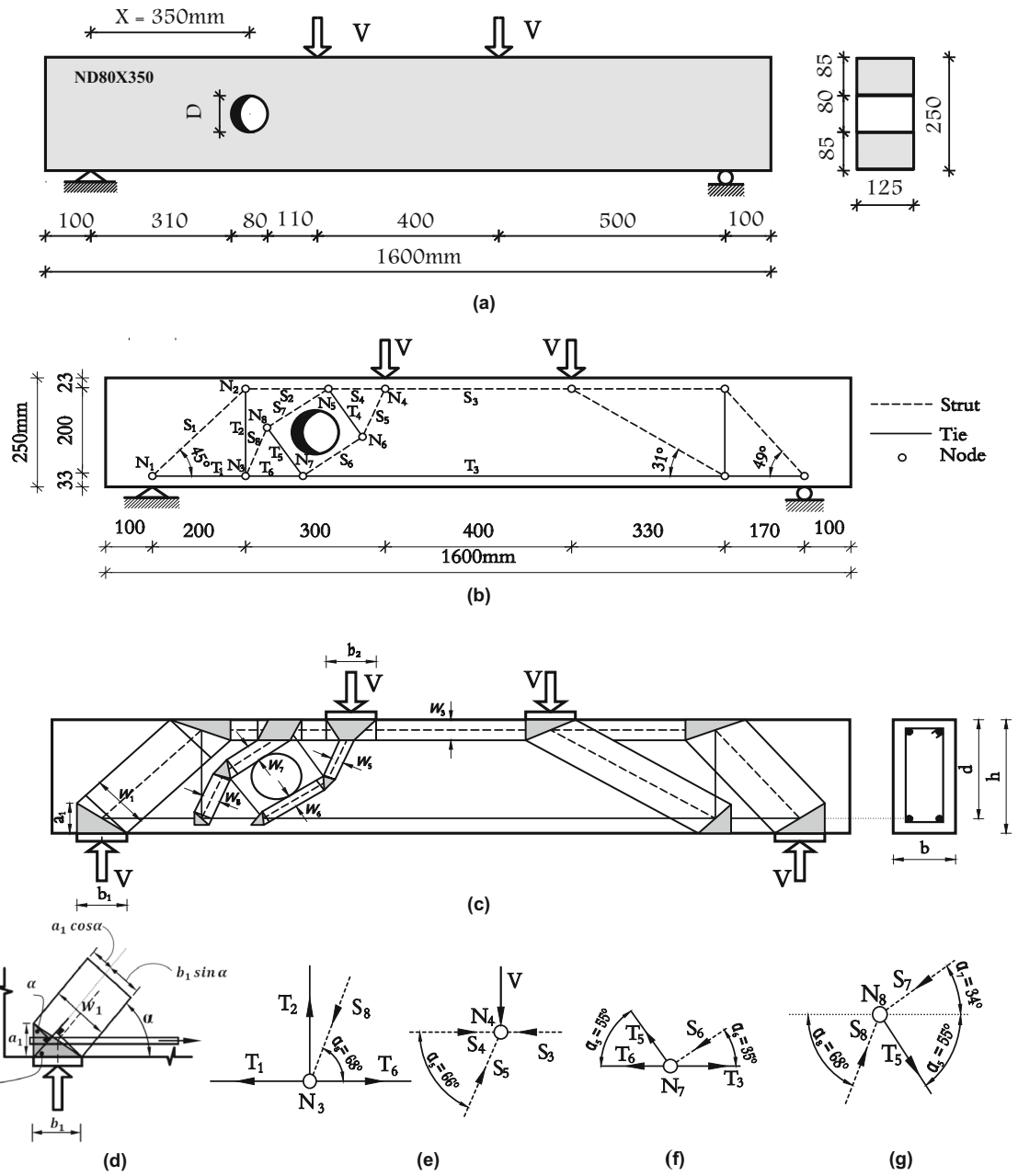

Fig. 1 Beam ND80X350. **a** Concrete dimensions and location of opening. **b** Details of the strut-and-tie model. **c** Visualization of strut widths. **d** Nodal zone N_1. **e** Equilibrium at nodes N_3 & N_4. **f** Equilibrium at nodes N_7. **g** Equilibrium at nodes N_8

Concrete Struts: There are three major geometric shapes for struts: *prismatic, bottle shaped,* and *compression fan* [6]. The strength of concrete in compression stress fields depends greatly on the multi-axial state of stress and disturbances from cracks and reinforcement. The effective compressive strength of the concrete in a strut f_{ce}^{s} is given by [1,5]:

$$f_{ce}^{s} = 0.85 f_c' \beta_s \quad \text{or} \quad 0.67 f_{cu} \beta_s$$

where β_s is the effectiveness factor of a concrete strut, which considers the stress conditions, strut geometry, and angle of cracking surrounding the strut. Table 1 adopts the β_s values of the ACI 318M-11 [1]. The *nominal compressive strength* of a concrete strut without longitudinal reinforcement F_{ns} shall be taken the smaller value of:

$$F_{ns} = f_{ce}^{s} A_{cs}$$

Table 3 The STM results compared with test results of ordinary beams Group B [7]

No.	Beam	P_{EXP} (kN)	Failure mode, Exp.	P_{STM} (kN)	Failure mode, STM	P_{STM}/P_{EXP}
1	S	120	Shear	70.68	Tension	0.600
2	ND80X350	100	Shear	70.70	Tension	0.707
3	ND80X150-s	100	Shear	70.70	Tension	0.707
4	ND80X250-s	110	Shear	70.83	Tension	0.644
5	ND100X350-s	105	Shear	70.53	Tension	0.672
6	HD80X150-s	115	Shear	70.80	Tension	0.616
7	HD100X350-s	115	Shear	70.55	Tension	0.613
Mean						0.651

N normal-strength concrete, *H* high-strength concrete, *D* diameter of opening, X = the distance between the center of opening to support, and s means small stirrups on top and bottom of opening

at the two ends of the strut, where A_{cs} is the cross-sectional area at one end of the strut and f_{ce}^{s} is the smaller of:

- The effective compressive strength of the concrete in the strut.
- The effective compressive strength of the concrete in the nodal zone.

The design of struts shall be based on $\Phi F_{ns} \geq F_{us}$, where Φ is the strength reduction factor and F_{us} is the factored strut force. In another form

$$\Phi \left(0.85 f_c' \beta_s\right) A_{cs} \geq F_{us}$$

Nodal Zones: The compressive strength of concrete of a nodal zone depends on the tensile straining from intersecting ties, confinements provided by compressive reactions and transverse reinforcement. The effective compressive strength of concrete in a nodal zone f_{ce}^{n} is [1,5]:

$$f_{ce}^{n} = 0.85 f_c' \beta_n \quad \text{or} \quad 0.67 f_{cu} \beta_n$$

where β_n is the effectiveness factor of a nodal zone and it is assumed as given in Table 2, ACI 318M-11 [1]. *The nominal compressive strength* of a nodal zone, F_{nn}, shall be

$$F_{nn} = f_{ce}^{n} A_{nz}$$

where f_{ce}^{n} is the effective compressive strength of concrete in the nodal zone and A_{nz} is the smaller of:

- The area of the face of the nodal zone on which F_u acts, taken perpendicular to the line of action of the strut force F_u.
- The area of a section through the nodal zone, taken perpendicular to the line of action of the resultant force on the section.

In smeared nodes, where the deviation of forces may be smeared or spread over some length, the check of stress is often not critical and it is only required to check the anchorage of the rebar. On the other hand, singular or concentrated nodes have to be carefully checked.

4 Simple Ordinary Beams Using STM: Verification Examples

To illustrate how to model and analyze RC ordinary beams with/without openings using the STM method, three groups of simple ordinary beams with/without openings that had been tested experimentally are chosen and examined. The tested groups are: *Group B* [7], *Group C* [8], and *Group D* [9]. The variables of (1) strengths of rebar and concrete, (2) specimen dimensions, (3) loading, (4) shear span-to-depth ratio, and (5) the amount of main and web reinforcement are considered.

Group B [7]: NSC and HSC Beams

Beam ND80X350: Fig. 1a shows a simple RC ordinary beam, ND80X350, with one unsymmetric circular opening. The beam was tested under two symmetric top point loads, and hence, the proposed STM is given in Fig. 1b. The model has six struts S_1–S_6, four ties T_1–T_4, and six nodes N_1–N_6. Two external top point loads are applied at nodes N_4. The ties T_1, T_3, and T_6 represent the main longitudinal steel, and the vertical reinforcement is represented by tie T_2. The numerical scheme of the beam is given in appendix A, from which the beam fails due to yielding of tension ties at a load, $P_{STM} = 70.7$ kN, whereas the experimental failure load $P_{EXP} = 100.0$ kN; thus, $P_{STM}/P_{EXP} \cong 0.70$.

The results of other beams of *Group B* have been obtained using the same numerical scheme of appendix A, and they are given in Table 3. The STM approach gives a mean value 0.651 of the experimental ultimate load. Based on experimental

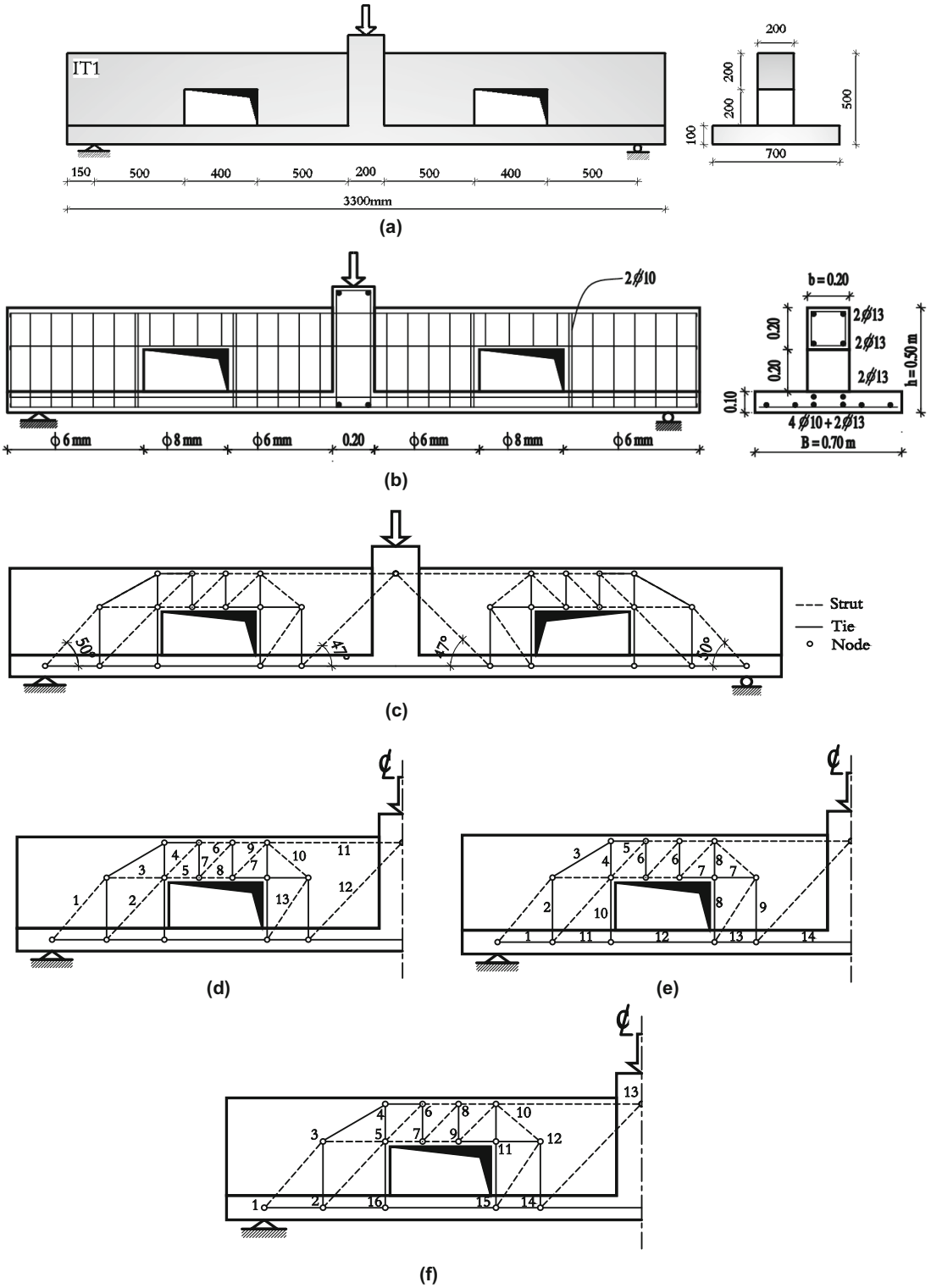

Fig. 2 Beam IT1. **a** Concrete dimensions and location of openings. **b** Details of reinforcement. **c** Details of the STM. **d** Strut labels for strut-and-tie model. **e** Tie labels for strut-and-tie model. **f** Node labels for strut-and-tie model

Table 4 The STM results compared with test results of ordinary beams Group D [9]

No.	Beam	$P_{EXP,\,kN}$	Failure mode, Exp.	$P_{STM,\,kN}$	Failure mode, STM	P_{STM}/P_{EXP}
1	IT1	314.67	Tension	211.28	Tension	0.700
2	IT4	154.02	Tension	98.46	Tension	0.640
3	IT8	256.02	Tension	212.83	Tension	0.831
Mean						0.724

data and the STM results, the presence of openings reduces the beam capacity.

Group D [9]: NSC Beams

Inverted T-beam IT1: Fig. 2a shows a simple RC ordinary beam with two symmetric rectangular openings and tested under one top point load. The beam reinforcement is shown in Fig. 2b, and the proposed STM is given in Fig. 2c. The model has 13 struts S_1–S_{13}, 14 ties T_1–T_{14}, and 16 nodes N_1–N_{16}. The external top point load is applied at nodes N_{13}. The tie T_1 and ties T_{11}–T_{14} represent the main longitudinal reinforcement. The numerical scheme of the beam is given in appendix B, from which the beam fails at a load, $P_{STM} = 211.28\,kN$, whereas the experimental failure load $P_{EXP} = 314.67\,kN$; thus, $P_{STM}/P_{EXP} \cong 0.70$.

The results of all other beams have been obtained and are given in Table 4. The STM approach gives a mean value 0.724 of the experimental ultimate load.

Group C [8]: NSC Beam

Beam with two rectangular openings (300 × 100 mm): Fig. 3a, b show a simple RC ordinary beam with two symmetric openings, 2-top point loads along with the proposed STM. The model has 26 compression struts S_1–S_{26}, 35 tension ties T_1–T_{35}, and 50 nodes N_1–N_{50}. The ties T_1, T_{26}–T_{34} represent the main longitudinal reinforcement, and the vertical reinforcement is represented by the other ties. With reference to Fig. 3, $h = 250\,mm$, $d = 210\,mm$, $b = 100\,mm$, $b_1 = 50\,mm$, and $b_2 = 100\,mm$. The shear span-to-depth ratio $(a/d) = (670/210) = 3.2$. The beam materials: $f'_c = 52\,MPa$, $f_y = 400\,MPa$, $f_{yv} = 240\,MPa$, A_s (4–10 mm bars) $= 314.16\,mm^2$, and $A_{sv} = 50.27\,mm^2$ per tie (one leg). The nominal shear force is $V_n = S_{16n} \sin\alpha_{16} = 22.04 \times \sin 59^o = 18.89\,kN$, $P_{STM} = 2V_n = 37.78\,kN$ and $P_{STM}/P_{EXP} = 37.78/41.00 = 0.92$.

5 Deep Beams Using STM Approach: Verification Examples

To illustrate how to model and analyze RC deep beams with openings using a STM method, *two tested groups A* [10] and *B* [11] of simple deep beams with openings are examined. The studied parameters are as follows: (1) strengths of rebar and concrete, (2) specimen dimensions, (3) loading, (4) shear span-to-depth ratio, and (5) the amount of main and web reinforcement. Finally, the obtained STM results are compared with the experimental results.

Group A [10]: NSC and HSC Simple and Continuous Deep Beams

Beam DSON3: Fig. 4 shows a simple RC deep beam with two symmetric rectangular openings, tested under one top point load. Figure 4c shows a proposed refined STM of the beam, whereas Fig. 4d shows a simplified STM; both models utilize inclined ties. The simplified model has five struts S_1–S_5, five ties T_1–T_5, and six nodes N_1–N_6. An external top point load is applied at node N_4. The ties T_1 and T_2 represent the main longitudinal steel, and the web reinforcement is represented by ties T_3 and T_4. The numerical scheme of the beam is given in appendix C. Alternative refined and simplified models that utilize vertical and horizontal ties are shown in Fig. 4f, g, respectively. The simplified model with the vertical and horizontal ties, Fig. 4g, is better than that with inclined ties, Fig. 4e, because it better reflects the reinforcement detailing of the beam, and therefore, it gives larger capacity, $P_{STM} = 130.0\,kN$. The experimental failure load, $P_{EXP} = 140.0\,kN$; hence, $P_{STM}/P_{EXP} \cong 0.93$.

Table 5 shows the results of other beams of *Group A*, where the STM approach gives a mean value of 0.785.

Group B [11]: NSC Simple Deep Beams

Table 6 shows the results of all beams of Group B [11]. The STM gives a mean value of 0.732 of the experimental ultimate load. The absence of web reinforcement in beam NO-0.3/4 caused a reduction in its capacity and ductility; the beam failed suddenly. The beams response significantly improved as a result of web reinforcement; the best advantage could be gained by reinforcing the beam above and below the opening.

6 3-D Nonlinear FEA of Ordinary Beams with Openings

6.1 Introduction

In order to predict the complete response of RC beams (displacements, strains and stresses, ultimate shear loads, failure modes, cracking pattern, etc.), a 3-D nonlinear FEA using

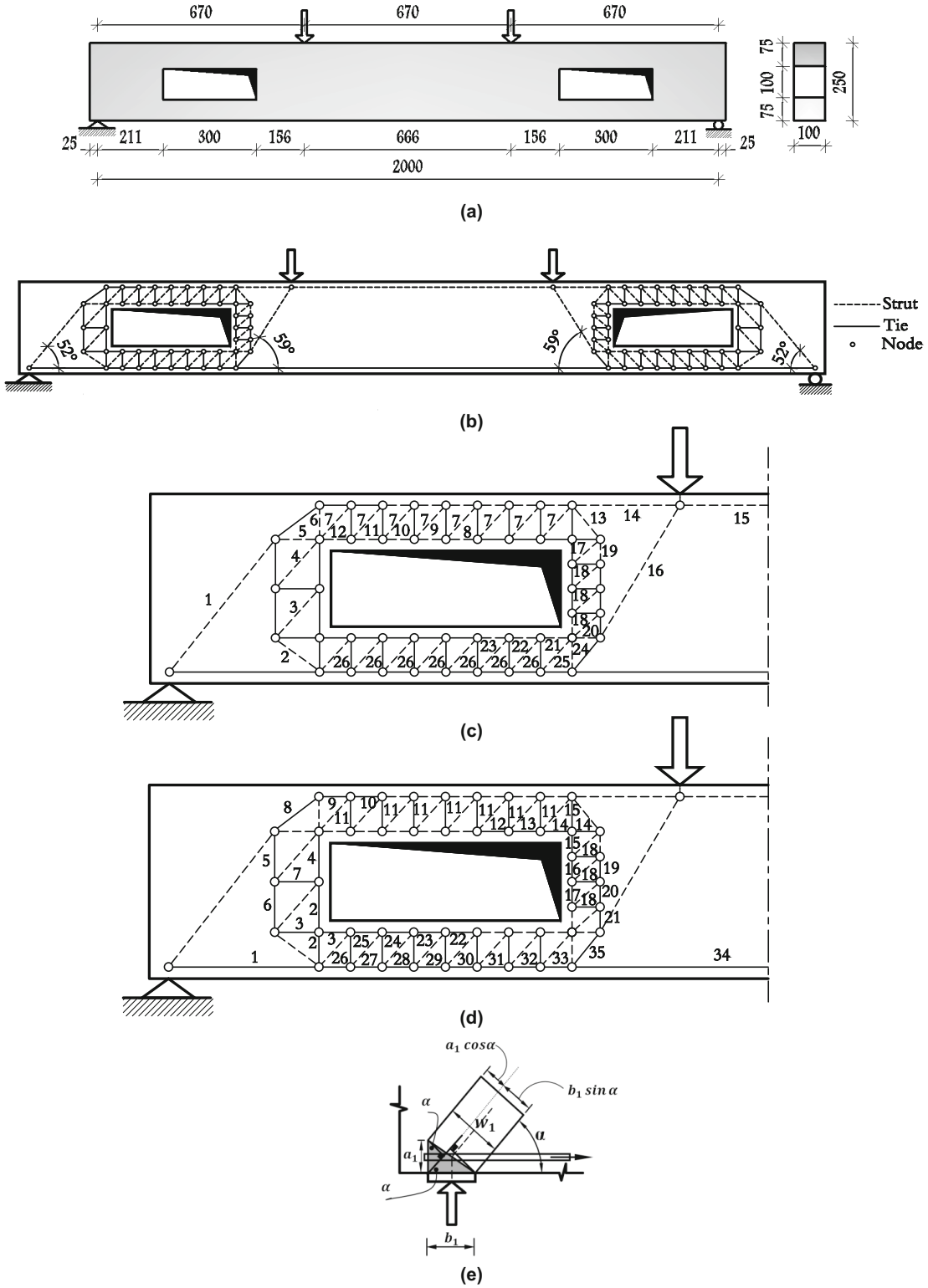

Fig. 3 Beam with rectangular openings (300 × 100 mm). **a** Concrete dimensions and location of opening. **b** Details of the STM. **c** Strut labels for strut-and-tie model. **d** Tie labels for strut-and-tie model. **e** Nodal zone at support

ANSYS-12 [4] is utilized. Concrete is modeled using a 3-D RC element SOLID65, capable of cracking in tension and crushing in compression. The main and web reinforcements are modeled using LINK8-3-D bar element within the concrete SOLID65. The program accounts for material nonlinearity of both steel and concrete.

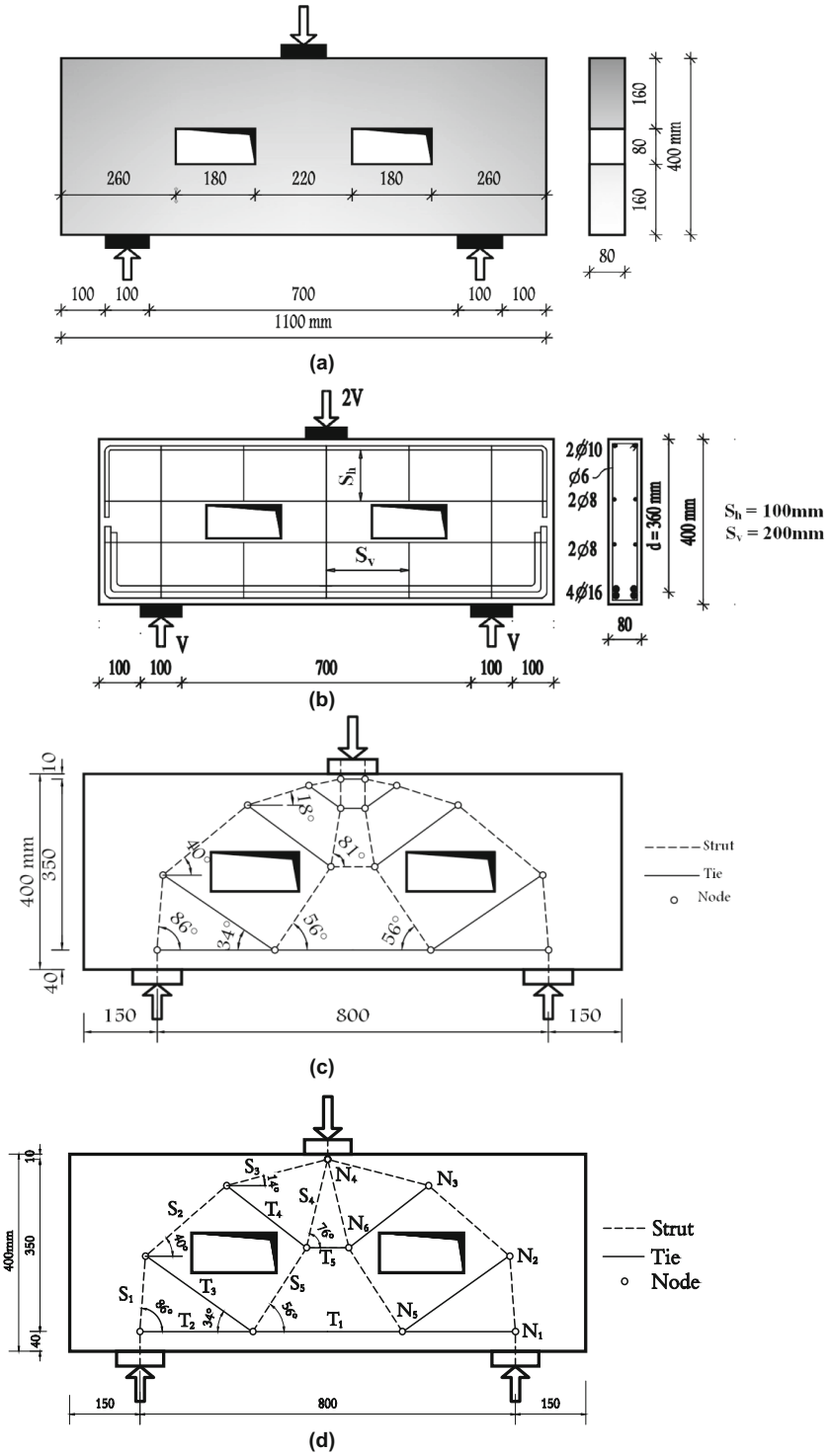

Fig. 4 Beam DSON3 Group A. **a** Concrete dimensions and location of opening. **b** Details of reinforcement. **c** Details of the proposed refined STM of beam DSON3 using inclined ties. **d** Details of the proposed simplified STM of beam DSON3 using inclined ties. **e** Visualization of strut widths using inclined ties of beam DSON3. **f** Alternative refined STM of beam DSON3 using vertical and horizontal ties. **g** Alternative simplified STM of beam DSON3 using vertical and horizontal ties. **h** Visualization of strut widths using vertical and horizontal ties of beam DSON3

6.2 Verification Group B [7]: Simple Beams with/Without Circular Openings

A nonlinear FEA has been performed for seven simple ordinary beams [7] with/without openings. The beam shown in Fig. 5 is discussed in detail next.

The 3-D nonlinear FEA aims to examine three different aspects: (1) initial cracking of the beam, (2) yielding of the steel reinforcement, and (3) the beam's strength limit state, which is recognized when convergence fails. In the analysis, four steel plates are used to model the supports and bearings of point loads, Fig. 5b. The point load is

Fig. 4 continued

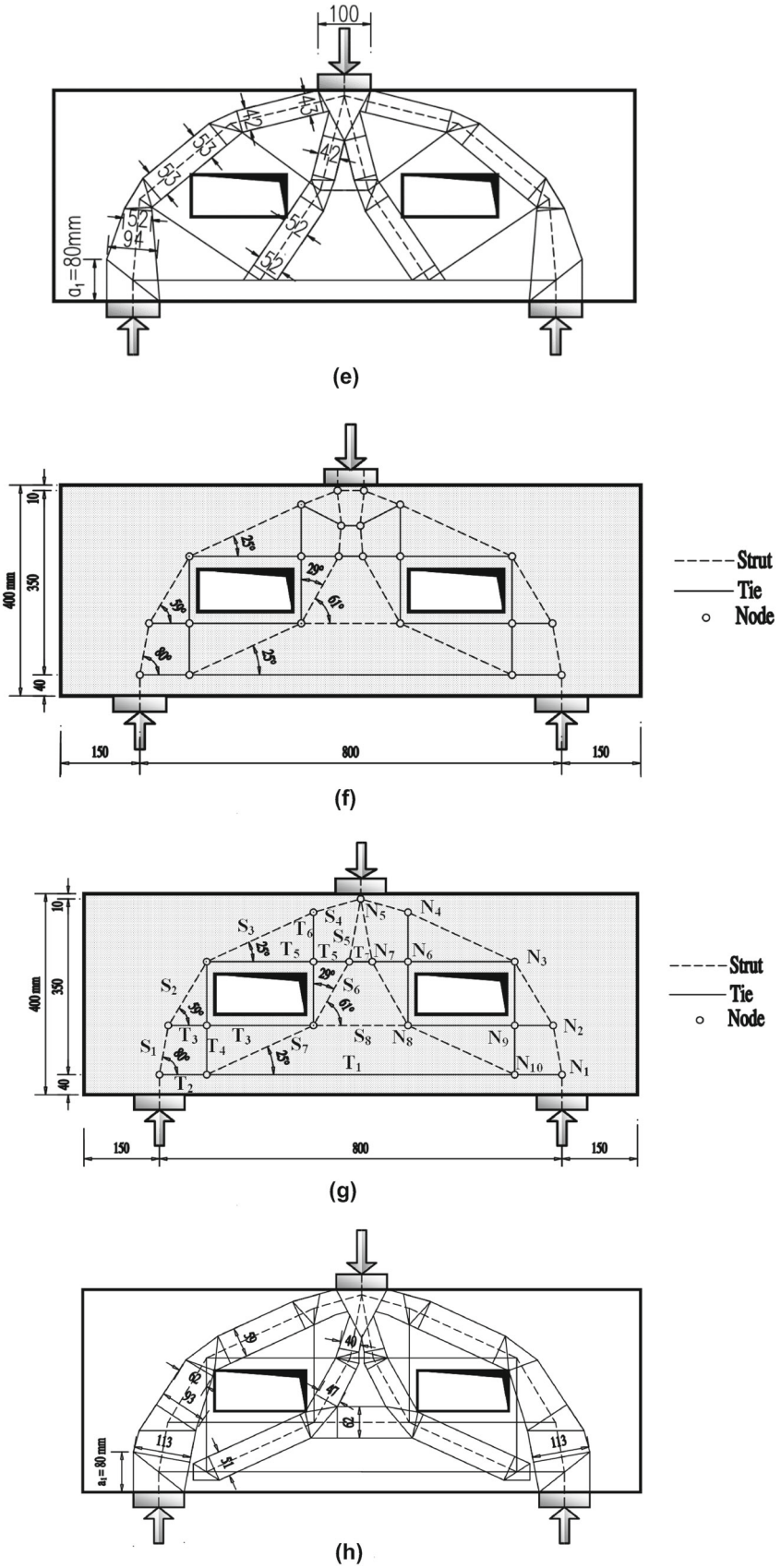

Table 5 The STM results compared with test results of deep beams Group A [10]

No.	Beam	$P_{EXP,\,kN}$	Failure mode, Exp.	$P_{STM,\,kN}$	Failure mode, STM	P_{STM}/P_{EXP}
1	DSON3	140	Opening failure	130.0	Opening failure	0.930
2	DSOH10	110	Opening failure	98.56	Opening failure	0.896
3	DCON3	220	Opening failure	176.43	Opening failure	0.801
4	DCOH2	360	Opening failure	280.12	Opening failure	0.778
5	DCOH8	290	Opening failure	150.31	Opening failure	0.518
Mean						0.785

Table 6 The STM results compared with test results of deep beams Group B [11]

No.	Beam	$P_{EXP,\,kN}$	Failure mode, Exp.	$P_{STM,\,kN}$	Failure mode, STM	P_{STM}/P_{EXP}
1	NO-0.3/4	240	Opening failure	212.32	Opening failure	0.885
2	NW1-0.3/4	420	Opening failure	305.16	Opening failure	0.727
3	NW2-0.3/4	580	Opening failure	317.45	Opening failure	0.547
4	NW3-0.3/4	620	Opening failure	490.18	Opening failure	0.791
5	NW7-0.3/4	720	Opening failure	510.47	Opening failure	0.709
Mean						0.732

applied at 5 nodes along the centerline of the steel plate, Fig. 5b.

The first flexural crack occurred in the constant bending moment (BM) region, Fig. 5f. Subsequent cracking occurred in this region as the load increased; then, the beam started to crack-out toward the supports, Fig. 5h, and diagonal tension cracks started to form, Fig. 5i, with excessive rate after yielding of reinforcement. The predicted and experimental cracking patterns of the beam at failure are shown in Fig. 5j. *Smeared cracks* are indicated by short lines, whereas *discrete cracks*, visualizing crushed concrete, are indicated by gray spots.

For all specimens, at about 19 % of the ultimate load, the first vertical flexural crack was formed in the region of the maximum BM. At about 40 % of the ultimate load, a sudden major inclined tension crack was formed almost in the middle part of the shear span. With increasing the load, the inclined cracks propagated backwards till they reached the beam bottom at the support block edges, Fig. 5h. In the meantime, the cracks propagated above the openings to the point load, and down the openings to the supports. With further increase in the load, the existing vertical flexural and inclined shear cracks were formed parallel to the original inclined cracks in the shear span, Fig. 5j. At about 99 % of the ultimate load, cracks (at the top and bottom corners of the rectangular opening or diagonally in case of circular opening, nearest to the load and support) increased and failure occurred in the opening region.

Table 7 shows the FEA results of the first flexural and diagonal cracking and ultimate load. The output of ANSYS of some tested beams is as shown in Figs. 5 and 6. For solid beam **S**, the normally expected distribution of principal stresses has been predicted. Compression stresses are concentrated along the load path. The tensile stresses are eliminated in the nonlinear FEA producing cracks in concrete, while tensile stresses are transferred to steel bars crossing this zone, Fig. 5e. In beams with openings, the load paths deviate around the openings; the concrete stresses are forced to deviate through narrow paths resulting in an increase in stress redistribution, Figs. 5e–6c. Increasing the concrete strength increases the load capacity. Higher compressive stresses occur at nodal zones (point loads and supports), while a reduction in the compressive stresses occurs in the inclined struts joining point loads and supports. The reduction is due diagonal cracks and web opening crossing the load path.

A comparison between the recorded experimental ultimate failure load $\mathbf{V_{u,Exp}}$ and the predicted failure load of the tested simple ordinary beams of Group B [7] calculated from the FEA $\mathbf{V_{u,FEM}}$ is given in Table 7. The mean value of the ratio $\mathbf{V_{u,FEM}/V_{u,Exp}}$ is 0.99, which demonstrates that the accuracy of the nonlinear FEA in estimating the nominal strength. Clear that the adopted nonlinear FEA provides a useful tool in understanding the behavior of simple NSC and HSC ordinary beams with and without openings.

6.3 Verification Group C [8]: Simple Beams W/Without Rectangular Openings

For two specimens (with/without openings) [8], at about 20–35 % of the ultimate load, the first vertical flexural cracks were formed in the region of the maximum bending moment. At about 40–70 % of the ultimate load, a sudden major inclined tension crack was formed almost in the middle part of the shear span. Upon increasing the load, the inclined cracks propagated backwards till they reached the beam bottom at the support block edges, Fig. 7d. In the meantime,

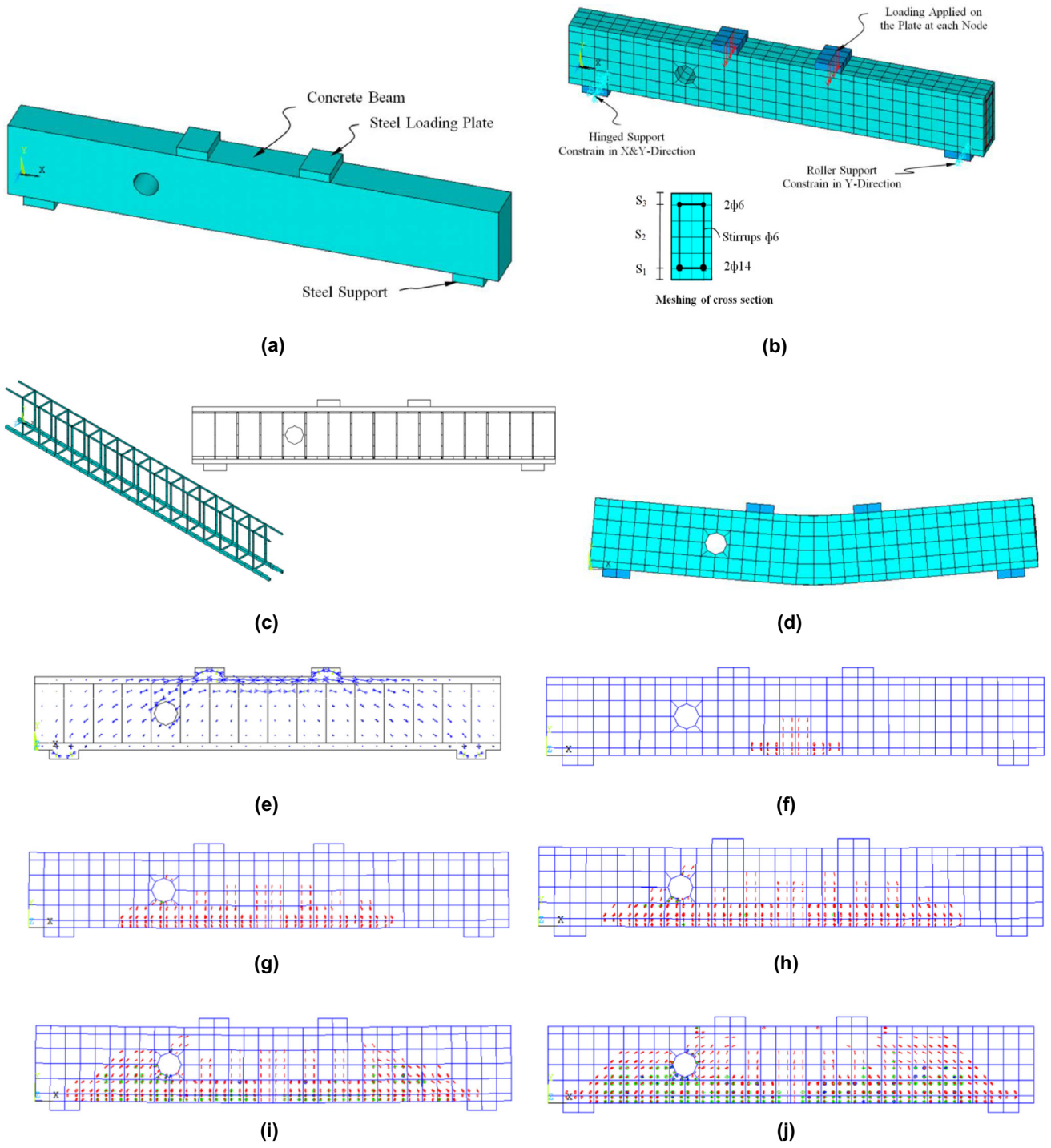

Fig. 5 Output of ANSYS-12 of beam ND80X350. **a** Beam model (volumes created in ANSYS). **b** Meshing of beam and cross section, applied loads and boundary conditions. **c** Reinforcement configurations. **d** Deformed shape. **e** Vector plots of principal stresses. **f** First cracks for flexure at load 19.40 kN. **g** Flexural cracks pattern. **h** First cracks for shear at load 41 kN. **i** Diagonal cracks pattern. **j** Cracks pattern at failure loads 100 kN

the cracks propagated above the openings to the point load, and down to the supports. With further increase in the load, the existing vertical flexural and inclined shear cracks were formed parallel to the original inclined cracks in the shear span, Fig. 7d. At 97–100 % of the ultimate load, cracks (at the top and bottom corners of the opening nearest to the load and support, respectively) increased and failure occurred in the opening region. The FEA results of the first flexural, diag-

Table 7 ANSYS versus experimental results of ordinary beams Group B [7]

No.	Beam	First cracking loads		Analytical ultimate load $2V_{u,\,FEM\,(kN)}$	Experimental ultimate load $2V_{u,Exp\,(kN)}$	$\frac{V_{crf}}{V_{u,FEM}}$	$\frac{V_{crs}}{V_{u,FEM}}$	$\frac{V_{u,FEM}}{V_{u,Exp}}$
		Flexure $2V_{crf\,(kN)}$	Shear $2V_{crs\,(kN)}$					
1	S	21.00	45.50	117.22	120.00	0.18	0.39	0.98
2	ND8X35	19.40	41.00	100.00	100.00	0.19	0.41	1.00
3	ND8X15-s	19.80	41.67	98.45	100.00	0.20	0.42	0.98
4	ND8X25-s	20.00	42.30	108.64	110.00	0.18	0.39	0.99
5	ND10X35-s	20.00	39.00	105.00	105.00	0.19	0.37	1.00
6	HD8X15-s	22.00	44.30	114.20	115.00	0.19	0.39	0.99
7	HD10X35-s	22.23	44.15	114.86	115.00	0.19	0.38	0.99
Average								0.99

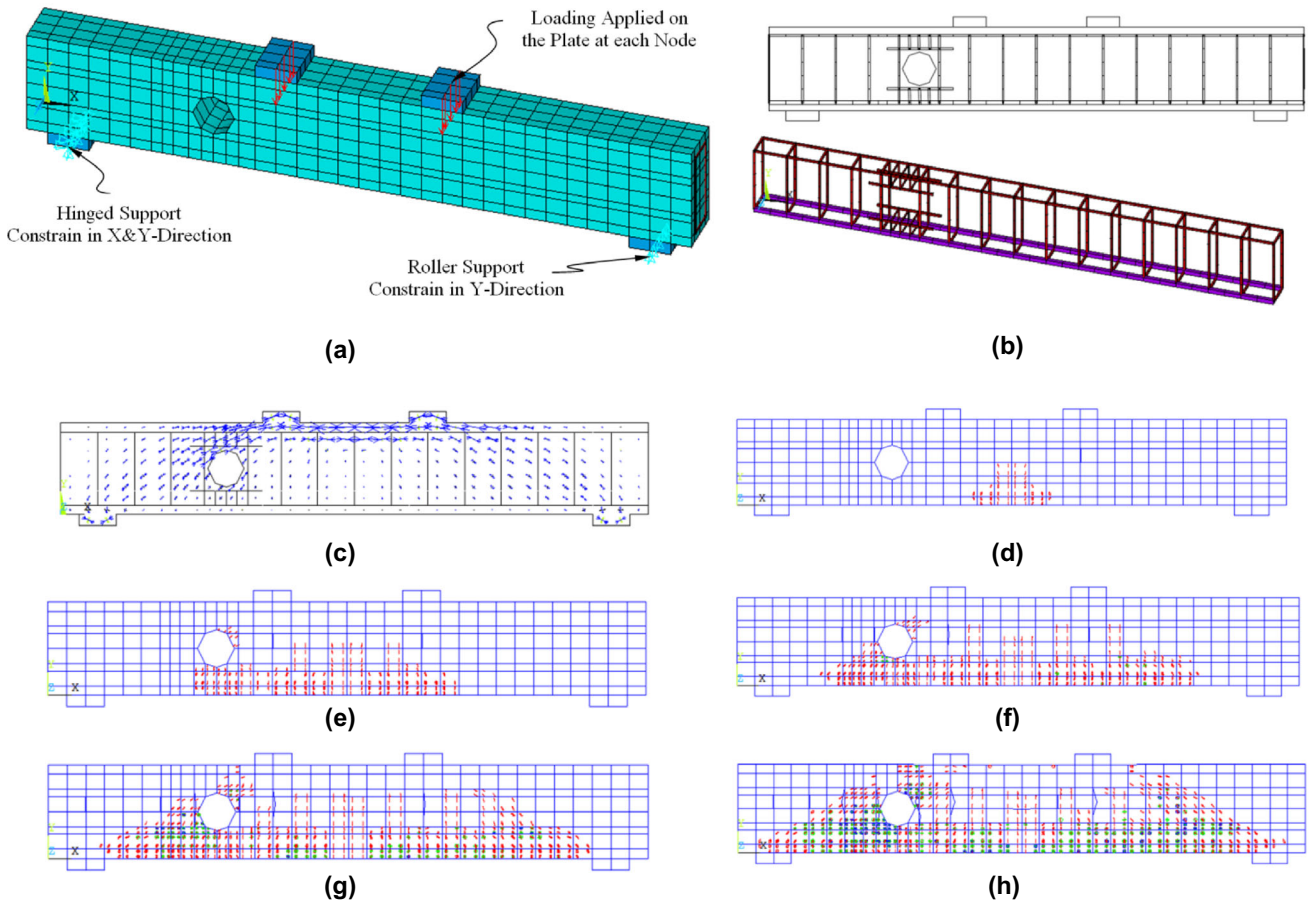

Fig. 6 Output of ANSYS-12 for beam ND100X350-s. **a** Applied loads and boundary conditions. **b** Reinforcement configurations. **c** Vector plots of principal stresses. **d** First cracks for flexure at load 20 kN. **e** Flexural cracks pattern. **f** First cracks for shear at load 39 kN. **g** Diagonal cracks pattern. **h** Cracks pattern at failure loads 105 kN

onal crack and ultimate loads of the solid beam are 17.87, 34 and 80.53 kN, respectively. The FEA results for the first flexural, diagonal crack, and ultimate loads of the beam with rectangular openings are 14.86, 33.40, and 42 kN, respectively. Figure 7 shows the output of ANSYS [4] of the beams with openings. The higher compressive stresses exist at nodal zones (point loads and supports), while a reduction in the compressive stresses takes place in the inclined struts joining the point loads and supports. This reduction is due to the diagonal cracks and the web opening crossing the load path.

To examine the accuracy of the 3-D nonlinear FEA, the obtained results are compared with test results of two beams

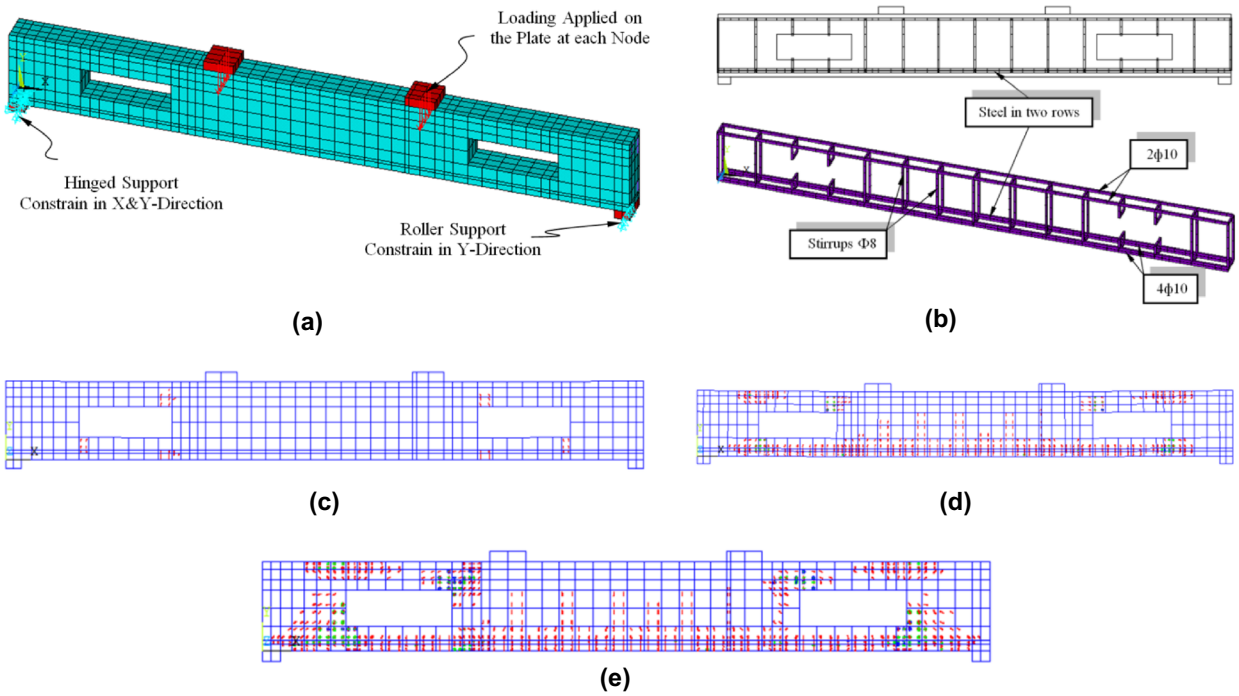

Fig. 7 Output of ANSYS-12 of beam with rectangular openings. **a** Applied loads and boundary conditions. **b** Reinforcement configurations. **c** First cracks for flexure at load 14.86 kN. **d** First cracks for shear at load 33.40 kN. **e** Cracks pattern at failure load 42 kN

Table 8 ANSYS versus experimental results of ordinary beams Group D [9]

No.	Beam	First cracking loads		Analytical ultimate load $2V_{u,\,FEM\,(kN)}$	Experimental ultimate load $2V_{u,\,Exp\,(kN)}$	$\frac{V_{crf}}{V_{u,FEM}}$	$\frac{V_{crs}}{V_{u,FEM}}$	$\frac{V_{u,FEM}}{V_{u,Exp}}$
		Flexure $2V_{crf\,(kN)}$	Shear $2V_{crs\,(kN)}$					
1	IT1	62.91	122.20	305.12	314.67	0.21	0.40	0.97
2	IT4	29.30	58.51	130.16	154.02	0.23	0.45	0.85
3	IT8	61.46	85.51	245.23	256.02	0.25	0.35	0.96
Average								0.93

in Group C [8]. The recorded experimental ultimate failure load $\mathbf{V_{u,Exp}}$ and the predicted failure load of the tested simple ordinary solid beam calculated from the FEA $\mathbf{V_{u,FEM}}$ are 83 and 80.53 kN, respectively. The recorded experimental ultimate failure load $\mathbf{V_{u,Exp}}$ and the predicted failure load of the tested simple ordinary beam with rectangular openings calculated from the FEA $\mathbf{V_{u,FEM}}$ are 41 and 42 kN, respectively. The mean value of the ratio $\mathbf{V_{u,FEM}/V_{u,Exp}}$ of the two ordinary beams is 0.985, which demonstrates that the nonlinear FEA provides accurate predictions of the ultimate load of beams, a useful tool in understanding the behavior of simple ordinary beams with/without openings.

6.4 Verification Group D [9]: Simple Beams with Rectangular Openings

For three specimens, similar responses to that of the two specimens of Group C, Sect. 6.3, but at about 23, 40, and 93 % of the ultimate load, respectively, were obtained. Table 8 shows the finite element results of the first flexural, diagonal crack and ultimate loads.

To examine the accuracy of the 3-D nonlinear FEA, the obtained results are compared with test results of the beams in Group D [9], Table 8. The mean value of the ratio $\mathbf{V_{u,FEM}/V_{u,Exp}}$ of ordinary beams is 0.93, which demonstrates that the nonlinear FEA provides accurate predictions of the ultimate load of ordinary beams.

7 3-D Nonlinear FEA of Deep Beams with Openings

7.1 Group A [10]: Simple/Continuous Deep Beams with Rectangular Openings, Figs. 8 and 9

First cracking: The first cracking occurs at the corner of the opening and it is noted that the opening affects the beams

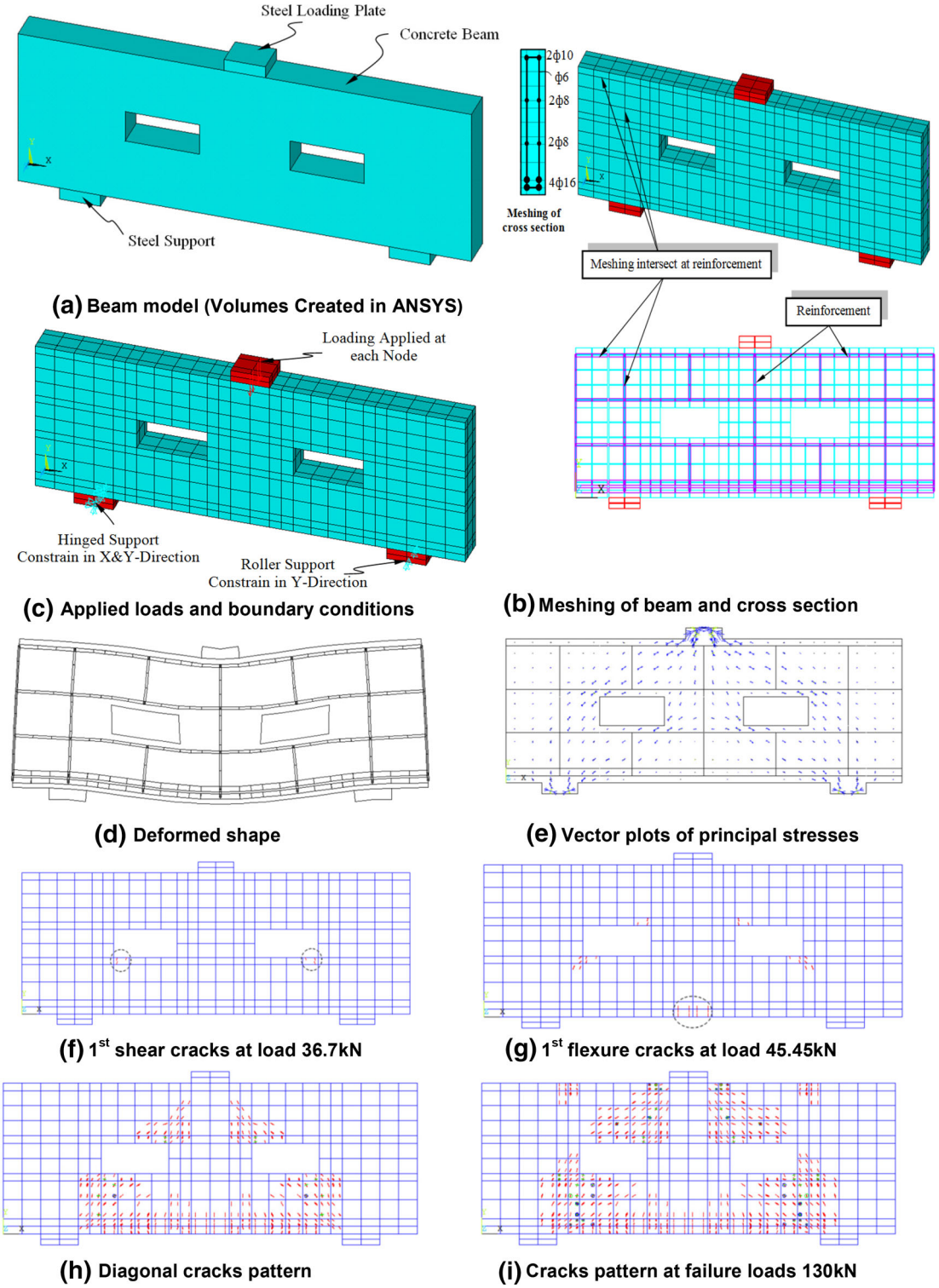

Fig. 8 Output of ANSYS-12 of beam DSON3

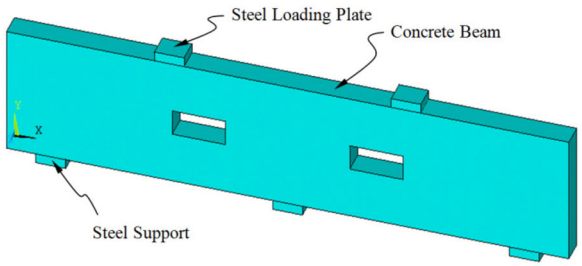

(a) Beam model

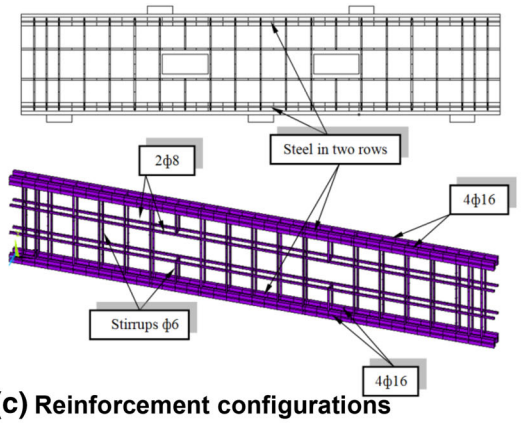

(c) Reinforcement configurations

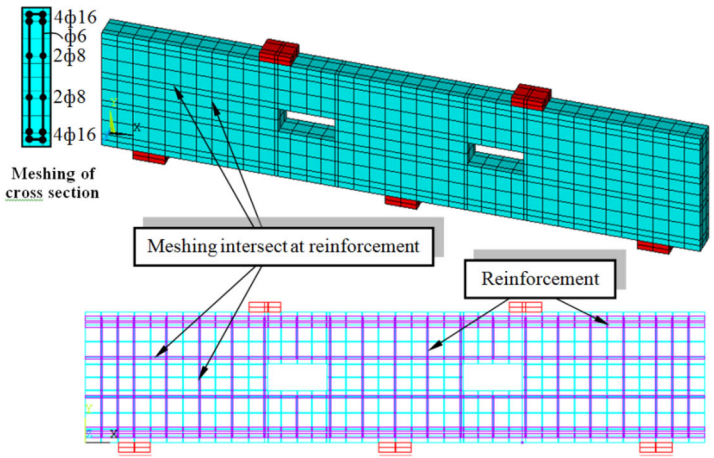

(b) Meshing of beam and cross section

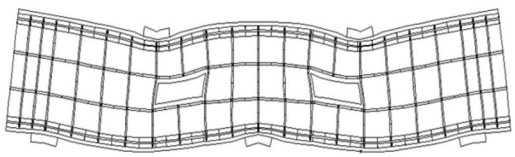

(d) Deformed shape

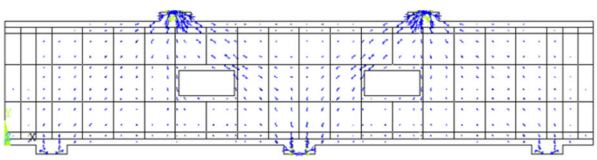

(e) Vector plots of principal stresses

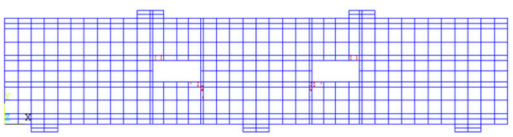

(f) 1st shear cracks at load 107.30kN

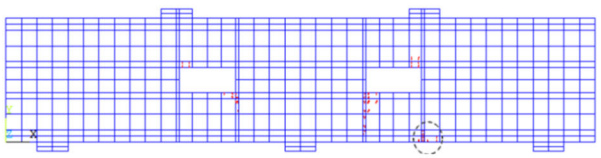

(g) 1st flexure cracks at load 109.80kN

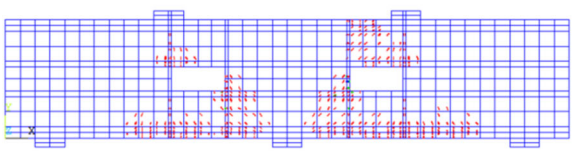

(h) Diagonal cracks pattern.

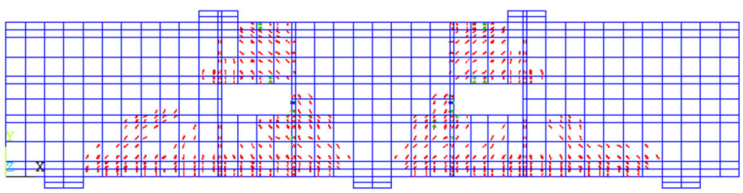

(i) Cracks pattern at failure load 218.58kN.

Fig. 9 Output of ANSYS-12 of beam DCON3

Table 9 ANSYS versus experimental results of deep beams Group A [10]

No.	Beam	First cracking loads		Analytical ultimate load $2V_{u,FEM\ (kN)}$	Experimental ultimate load $2V_{u,Exp\ (kN)}$	$\frac{V_{crs}}{V_{u,FEM}}$	$\frac{V_{crf}}{V_{u,FEM}}$	$\frac{V_{u,FEM}}{V_{u,Exp}}$
		Shear $2V_{crs\ (kN)}$	Flexure $2V_{crf\ (kN)}$					
1	DSON3	36.70	45.45	130.00	140	0.28	0.35	0.93
2	DSOH10	29.20	35.60	105.00	110	0.28	0.34	0.95
3	DCON3	107.30	109.80	218.58	220	0.49	0.50	0.99
4	DCOH2	158.70	172.50	345.00	360	0.46	0.50	0.96
5	DCOH8	115.00	135.80	285.00	290	0.40	0.48	0.98
Average								0.96

Table 10 ANSYS versus experimental results of deep beams Group B [11]

No.	Beam	Experimental	Analytical	$\frac{V_{u,FEM}}{V_{u,Exp}}$
		Ultimate load $2V_{u,Exp\ (kN)}$	Ultimate load $2V_{u,FEM\ (kN)}$	
1	NO-0.3/4	240	238.00	0.99
2	NW1-0.3/4	420	410.00	0.98
3	NW2-0.3/4	580	573.00	0.99
4	NW3-0.3/4	620	615.00	0.99
5	NW7-0.3/4	720	685.00	0.95
Average				0.98

stress trajectories drastically, where zones of tension stresses are formed around the left upper corner of the opening (load side) and the lower corner on the same diagonal, so first cracking occurs at this corner of opening and it is a shear crack, Figs. 8g and 9g. Inversely, in ordinary beams, first crack occurs in the constant moment region, and it is a flexural crack (vertical crack). *Behavior beyond first cracking:* In the nonlinear region of the response, subsequent cracking occurs as the load increases. Cracking increases out toward the supports and flexural cracking (vertical cracks) begins in the constant moment region, Fig. 8g. Also, diagonal tension cracks begin to form in the model, Fig. 8h, and increase after yielding of reinforcement. The predicted and experimental cracking patterns of the beams at failure are shown in Figs. 8i and 9i.

For all specimens, at about 43 % of the ultimate load, the first vertical flexural cracks were formed in the region of the maximum **BM**. At about 38 % of the ultimate load, a sudden major inclined tension crack was formed almost in the middle part of the shear span. Increasing the load, the inclined cracks propagated backwards till they reached the beam bottom at the support block edges, Fig. 8h. In the meantime, the cracks propagated above openings to point load and down to supports. Further increase in the load, the existing vertical flexural, and inclined shear cracks were formed parallel to the original inclined cracks in the shear span, Fig. 8i. At 96 % of the ultimate load, cracks (at the top and bottom corners of the opening nearest to the load and support, respectively) increased and failure occurred in the opening region.

Table 9 shows the FEA results for the first diagonal, flexural cracking, and ultimate loads. Figures 8 and 9 show ANSYS output for beams DSON3 and DCON3, respectively. In which, the normally expected distribution of principal stresses has been predicted. Compression stresses are concentrated along the load path. The tensile stresses are eliminated in the nonlinear analysis producing cracks in concrete, while tensile stresses are transferred to the steel bars crossing this zone. For beams having openings, the load path is deviated around the opening, the concrete stresses are forced to deviate through narrow paths, and the stress redistribution increases, Figs. 8e and 9e. Increasing the concrete strength increases the load capacity. Higher compressive stresses are found at the nodal zones (loads and supports), while a reduction in the compressive stresses occurs in the inclined struts joining the point loads and supports.

To examine the accuracy of the nonlinear FEA, the obtained results are compared with tested beams in Group A [10], Table 9. A mean value 0.96 of $\mathbf{V_{u,FEM}/V_{u,Exp}}$ demonstrates that the nonlinear FEA provides accurate prediction of the ultimate load of deep beams with openings.

7.2 Group B: Simple Beams with Rectangular Openings

Also, to examine the accuracy of the nonlinear FEA, the obtained results are compared with the measured values of the tested beams in Group B [11], Table 10, with a mean value 0.98 of $\mathbf{V_{u,FEM}/V_{u,Exp}}$. Figure 10 shows the output of ANSYS for beam NW7-0.3/4.

8 Summary and Conclusions

In this paper, the STM approach has been used to predict the capacity of RC shallow/deep beams with openings subjected to different loading and boundary conditions. Verification examples tested by others have been modeled and analyzed

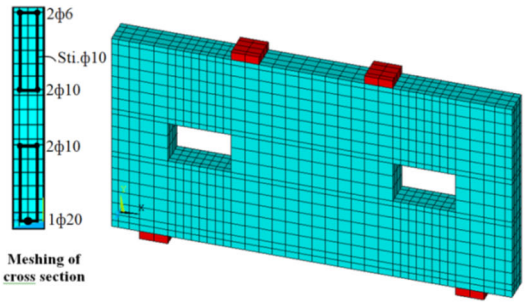

(a) Meshing of beam and cross section

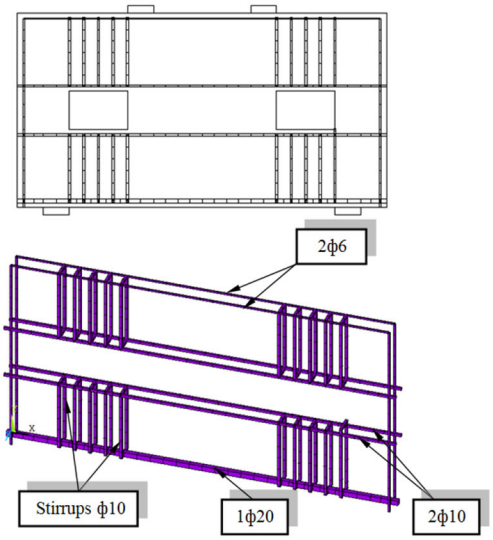

(b) Reinforcement configurations

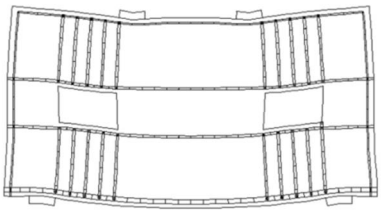

(c) Deformed shape

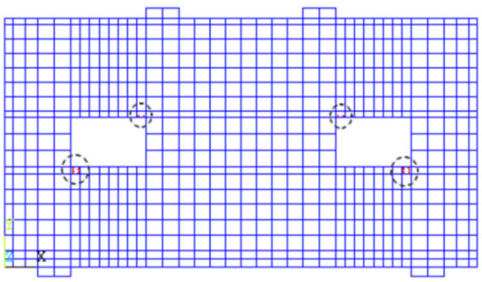

(d) 1st Cracks for shear at load 260kN

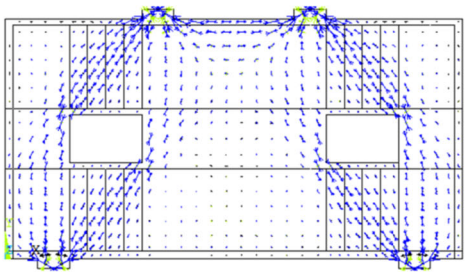

(e) Vector plots of principal stresses

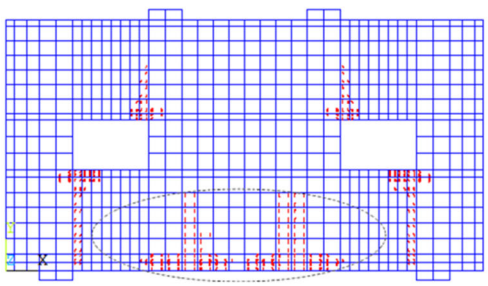

(f) Flexure cracks pattern after appearance shear cracks

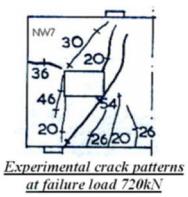

Experimental crack patterns at failure load 720kN

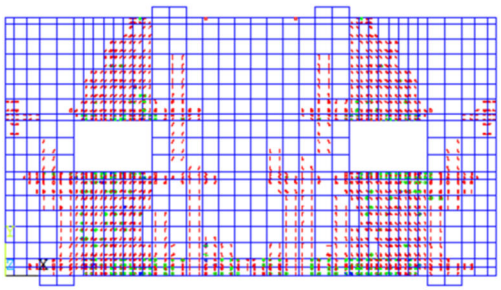

(g) FE Cracks pattern at failure load 685kN

Fig. 10 Output of ANSYS-12 of beam NW7-0.3/4

by proposing STMs, utilizing elastic principal stress trajectories from FEA. Three-dimensional nonlinear FEA has been conducted to predict the ultimate capacity of the aforementioned beams. The finite element predictions are very satisfactory when compared with the test results. From the applications of both the STM method and the 3-D nonlinear FEA presented here, the following conclusions can be drawn:

1. The STM gives reasonable lower bound estimate of the load carrying capacity of RC ordinary/deep beams with openings.
2. The 3-D nonlinear FEA of simple and continuous NSC and HSC ordinary/deep beams with openings yields accurate predictions of both the ultimate load and the complete response than the STM.
3. For deep beams, openings affect the stress trajectories drastically; zones of tension stresses are formed around the upper and lower corners of the opening (nearest to the load and supports, respectively) of the same diagonal. These shear cracks occur, in general, in the beam's shear span. Cracking increases with increasing the load in the shear span and propagates toward the midspan (flexural and vertical cracks).
4. For all considered deep beams with openings, a diagonal shear failure occurred in the shear span or around the upper and lower corners of openings (nearest to load and supports, respectively) of the same diagonal before yielding of the longitudinal rebar.
5. For all considered ordinary beams with openings, a diagonal shear failure occurred at corners of tension zones of opening, before the yielding of the longitudinal rebar.
6. Similar failure modes are obtained for both HSC and NSC shallow/deep beams.
7. The FEA solutions show that increasing the concrete strength results in an increase in the cracking and ultimate strength.
8. The obtained numerical results of RC beams show that the variation in the opening size has a significant effect on the ultimate load capacity.
9. The most favorable opening shape is the circular (minimum stress deviation).

Appendix A: Numerical Scheme of Beam ND80X350, Fig. 1

1. Input data:

With reference to Fig. 1, $h = 250\,\text{mm}$, $d = 217\,\text{mm}$, $b = 125\,\text{mm}$, the width of the bearing plates $b_1 = b_2 = 100\,\text{mm}$, and the opening diameter = 80 mm. The shear span-to-depth ratio $(a/d) = (500/217) = 2.3$. For the beam materials: the concrete cylinder strength $f'_c = 28.93\,\text{MPa}$ (NSC), the yield stress of longitudinal steel $f_y = 450\,\text{MPa}$, the yield stress of vertical ties $f_{yv} = 250\,\text{MPa}$, the area of the main steel A_s (2–14 mm bars) = 307.88 mm^2, the area of the secondary steel A'_s(2–6 mm bars) = 56.57 mm^2, and the area of vertical ties $A_{sv} = 141.37\,\text{mm}^2$ per tie (2-legs per tie).

2. The internal lever arm, L_d:

The term a_1 (height of node N_1, Fig. 1c, d) is $a_1 = n\emptyset_{\text{bars}} + 2c + (n-1)\,s = 1 \times 14 + 2 \times 26 + 0 = 66\,\text{mm}$. From equilibrium, $T_3 = S_3$; thus, $\text{Asf}_y = 0.85\,f'_c b w_3$ or $307.88 \times 450 = 0.85 \times 28.93 \times 125 \times w_3$ which gives $w_3 = 45.10\,\text{mm}$. Thus, $L_d = h - 0.5\,(a_1 + w_3) = 194.45\,\text{mm}$.

3. Width of struts:

The width of strut S_1 is obtained from the width of the bearing plate and the width of tie T_1, Fig. 1d:

$$w_1 = a_1 \cos\alpha + b_1 \sin\alpha = 66\cos 45 + 100 \sin 45 = 117.38\,\text{mm}.$$

The width of struts S_2 and S_4 can be assumed equal to w_3 for simplicity, i.e., $w_2 \cong w_3 \cong w_4 \cong a_2 = 45.10\,\text{mm}$. The width of struts S_5–S_8 can be determined by developing a realistic geometry of the struts as they extend from the nodes, Fig. 1c. For S_5–S_8, the following is assumed; $w_5 = w_6 = 27\,\text{mm}$ and $w_7 = w_8 = 38\,\text{mm}$; this is the maximum available width around the opening.

4. STM forces:

Assuming that the reinforcing bars (tension ties T_2 and T_3) will reach their yield strength and from equilibrium of the model nodes, the following relations can be written:

$$T_{2n,\max} = A_{st2} f_{yv} = A_{sv2} f_{yv} = 141.37 \times 250 = 35.34\,\text{kN and}$$
$$T_{3n,\max} = A_{st3} f_y = 307.88 \times 450 = 139\,\text{kN. Try } T_{2n} = T_{2n,\max} = 35.34\,\text{kN}$$

where $T_{in,\max}$ is the nominal strength of tie i when reaching its yield strength. From equilibrium,

Node 2:

$$S_{1n} = \frac{T_{2n,\max}}{\sin\alpha_1} = \frac{35.34}{\sin 45} = 50\,\text{kN and } S_{2n} = S_{1n}\cos\alpha_1 = 50 \times \cos 45^{\circ} = 35.40\,\text{kN}$$

Node 1:

$$T_{1n} = S_{1n}\cos\alpha_1 = 50 \times \cos 45^{o} = 35.40\,\text{kN} \quad \text{and}$$
$$V_n = S_{1n}\sin\alpha_1 = 50 \times \sin 45^{o} = 35.35\,\text{kN}$$

Node 3, Fig. 1e:

$$S_{8n} = \frac{T_{2n,\max}}{\sin\alpha_8} = \frac{35.34}{\sin 68} = 38.12\,\text{kN}$$
$$T_{6n} = T_{1n} + S_{8n}\cos\alpha_8 = 35.40 + 38.12\cos 68 = 49.68\,\text{kN}$$

Node 8, Fig. 1g:

$$S_{8n}\cos\alpha_8 = S_{7n}\cos\alpha_7 - T_{5n}\cos\alpha_5 \quad \text{or} \quad 38.12\cos 68 = S_{7n}\cos 34 - T_{5n}\cos 55 \tag{1}$$
$$S_{8n}\sin\alpha_8 = S_{7n}\sin\alpha_7 + T_{5n}\sin\alpha_5 \quad \text{or} \quad 38.12\sin 68 = S_{7n}\sin 34 + T_{5n}\sin 55 \tag{2}$$

Solving Eqs. 1 and 2 yields $S_{7n} = 31.97\,\text{kN}$ and $T_{5n} = 21.32\,\text{kN}$

Node 7, Fig. 1f:

$$S_{6n} = \frac{T_{5n}\sin\alpha_5}{\sin\alpha_6} = \frac{21.32\sin 55^{o}}{\sin 35} = 30.45\,\text{kN} \quad \text{and}$$
$$T_{3n} = S_{6n}\cos\alpha_6 + T_{5n}\cos\alpha_5 + T_{6n} = 30.45\cos 35 + 21.32\cos 55 + 49.68 = 86.85\,\text{kN} < T_{3n,\max}\ (\text{Okay})$$

Node 5:

$$T_{4n} = \frac{S_{7n}\sin\alpha_7}{\sin\alpha_4} = \frac{31.97\sin 34^{o}}{\sin 56} = 21.56\,\text{kN} \quad \text{and}$$
$$S_{4n} = S_{7n}\cos\alpha_7 + T_{4n}\cos\alpha_4 + S_{2n} = 31.97\cos 34 + 21.56\cos 56 + 35.40 = 73.96\,\text{kN}$$

Node 4, Fig. 1e:

$$S_{3n} = S_{4n} + S_{5n}\cos\alpha_5 = 73.96 + 28.68\cos 66 = 89.70\,\text{kN}$$

$$V_n = S_{5n}\sin\alpha_5 = 38.68\sin 66 = 35.34\,\text{kN} \quad \text{and}$$
$$P_{STM} = 2V_n = 70.70\,\text{kN}$$

5. Checking of stress limits:
(a) Concrete Struts: Knowing that $f'_c = 28.93\,\text{MPa}$, the term $\left(f_{ce} = 0.85 f'_c \beta\right)$ will be:

$$f_{ce}^{sj} = 0.85 f'_c \beta_{sj} = 0.85 \times 28.93 \times 1.00 = 24.59\,\text{MPa} \quad \text{for Strut } S_2,\ S_3,\ S_4,\ S_6, \quad \text{and} \quad S_7$$

$$f_{ce}^{sj} = 0.85 f'_c \beta_{sj} = 0.85 \times 28.93 \times 0.80 = 19.67\,\text{MPa} \quad \text{for Struts } S_1,\ S_5, \text{ and } S_8$$
$$f_{ce}^{ni} = 0.85 f'_c \beta_{ni} = 0.85 \times 28.93 \times 0.80 = 19.67\,\text{MPa} \quad \text{for Nodes } N_1,\ N_2,\ N_5,\ N_6 \text{ and } N_8$$
$$f_{ce}^{ni} = 0.85 f'_c \beta_{n4} = 0.85 \times 28.93 \times 0.60 = 14.75\,\text{MPa} \quad \text{for Node } N_3 \text{ and } N_7$$
$$f_{ce}^{n4} = 0.85 f'_c \beta_{n4} = 0.85 \times 28.93 \times 1.00 = 24.59\,\text{MPa} \quad \text{for Node } N_4$$

Upon substituting in $S_{jn,\max} = f_{ce}^{sj} b w_j$ and comparing the results with S_{jn}, the following is obtained:

$$S_{1n,\max} = f_{ce}^{s1} b w_1 = 19.67 \times 125 \times 117.38 = 288.61\,\text{kN} > S_{1n} = 50\,\text{kN}$$
$$S_{2n,\max} = f_{ce}^{s2} b w_2 = 24.59 \times 125 \times 45.10 = 138.63\,\text{kN} > S_{2n} = 35.40\,\text{kN}$$
$$S_{3n,\max} = f_{ce}^{s3} b w_3 = 24.59 \times 125 \times 45.10 = 138.63\,\text{kN} > S_{3n} = 89.70\,\text{kN}$$
$$S_{4n,\max} = f_{ce}^{s4} b w_4 = 24.59 \times 125 \times 45.10 = 138.63\,\text{kN} > S_{4n} = 73.96\,\text{kN}$$
$$S_{5n,\max} = f_{ce}^{s5} b w_5 = 19.67 \times 125 \times 25.00 = 61.47\,\text{kN} > S_{5n} = 38.68\,\text{kN}$$
$$S_{6n,\max} = f_{ce}^{s6} b w_6 = 24.59 \times 125 \times 27.00 = 82.99\,\text{kN} > S_{6n} = 30.45\,\text{kN}$$
$$S_{7n,\max} = f_{ce}^{s7} b w_7 = 24.59 \times 125 \times 38.00 = 82.99\,\text{kN} > S_{7n} = 31.97\,\text{kN}$$
$$S_{8n,\max} = f_{ce}^{s8} b w_8 = 19.67 \times 125 \times 38.00 = 82.99\,\text{kN} > S_{8n} = 38.12\,\text{kN}$$

(b) Nodes:
The capacity of a node is calculated by finding the product of the limiting compressive stress in the node region and the cross-sectional area of the member at the node interface.

Node N_1, Fig. 1d: Knowing that: $f_{ce}^{n1} = 0.85 f'_c \beta_{n1} = 19.67\,\text{MPa}$ (at Node N1)

$$S_{1n} \le \left(0.85 f'_c\right) \beta_{n1} w_1 b \text{ or } f_{ce}^{n1} w_1 b = 19.67 \times 117.38 \times 125 = 288.61\,\text{kN} > S_{1n}$$
$$V_n \le \left(0.85 f'_c\right) \beta_{n1} b_1 b \text{ or } f_{ce}^{n1} b_1 b = 19.67 \times 100 \times 125 = 245.88\,\text{kN} > V_n$$
$$T_{1n} \le \left(0.85 f'_c\right) \beta_{n1} a_1 b \text{ or } f_{ce}^{n1} a_1 b = 19.67 \times 66 \times 125 = 162.28\,\text{kN} > T_{1n}$$

Node N_4: Knowing that: $0.85 f'_c \beta_{n4} = f_{ce}^{n4} = 24.59$ MPa (at Node N4)

$$S_{3n} \le \left(0.85 f'_c\right) \beta_{n4} a_2 b \text{ or } f_{ce}^{n4} w_3 b = 24.59 \times 45.10 \times 125 = 138.63\,\text{kN} > S_{3n}$$

$$S_{4n} \le \left(0.85 f'_c\right) \beta_{n4} w_4 b \text{ or } f_{ce}^{n4} w_4 b = 24.59 \times 45.10 \times 125 = 138.63\,\text{kN} > S_{4n}$$

$$S_{5n} \le \left(0.85 f'_c\right) \beta_{n4} w_5 b \text{ or } f_{ce}^{n4} w_6 b = 24.59 \times 25.00 \times 125 = 76.84\,\text{kN} > S_{5n}$$

$$V_n \le \left(0.85 f'_c\right) \beta_{n4} b_2 b \text{ or } f_{ce}^{n4} b_2 b = 24.59 \times 100.0 \times 125 = 307.40\,\text{kN} > V_n$$

Nodes N_2, N_3, N_5, N_6, N_7, and N_8 are smeared, and therefore, their check is not necessary. Based on the recommendations of past researchers [12], it is unnecessary to apply the bonding stresses from a developed bar to the back face of a CCT node. Therefore, only directly applied stresses, such as those due to bearing of a plate or an external indeterminacy, are applied to the back face of CCT nodes and checked with the 0.80 effectiveness factor.
The safe solution yields a nominal shear force $V_n = 35.34$ kN and $P_{STM} = 2V_n = 70.70$ kN.

Appendix B: Numerical Scheme of Inverted T-beam IT1, Fig. 2

Input data:
With reference to Fig. 2, $h = 500$ mm, $d = 450$ mm, $b = 200$ mm, $b_1 = b_2 = 100$ mm, and the opening size is 200 × 400 mm. The shear span-to-depth ratio $(a/d) = (1500/450)$=3.33. For the beam materials: f'_c=36.20 MPa, f_y=538.8 MPa for 10 mm bars, f_y=513.6 MPa for 13 mm bars, $f_{yv} = 355.2$ MPa for 6 mm bars, $f_{yv} = 321.8$ MPa for 8 mm bars, and $A_s = 530.93$ mm^2 for 4–13 mm bars.

The internal lever arm, Ld:

The term a_1 (height of node N_1) is equal to the height of flange. Thus, $a_1 = 100$ mm. Since $T_14 = S_11$ or $\text{Asf}_y = 0.85 f'_c b a_2$ or $530.93 \times 513.6 = 0.85 \times 36.2 \times 200 \times a_2$ which gives $a_2 = 44.31$ mm, thus $L_d = h - 0.5\,(a_1 + a_2) = 427.85$ mm

Width of struts:

The widths of struts S_1, S_6, S_9, S_{11}, and S_{11} are calculated based on the size of bearing plates dimensions and the widths of the tie T_1 and the top strut S_{11} as follows:-

Table 11 STM forces of beam IT1, Fig. 2

Model label	Force (kN)	C or T	Model label	Force (kN)	C or T
1	154.95	C	8	1.43	C
2	168.10	C	9	213.10	C
3	111.50	C	10	29.1	C
4	161.91	C	11	303.29	C
5	113.60	C	12	161.93	C
6	100.92	C	13	163.00	C
7	162.44	C	–	–	–

T tension (tie), *C* compression (strut)

$$w_1 = a_1 \cos\alpha + b_1 \sin\alpha \text{ or } w_1 = 100 \times \cos 40 + 100 \sin 40 = 140.88\,\text{mm}$$

$$w_6 = w_9 = w_{11} = a_2 = 44.31\,\text{mm and } w_{12} = 95\,\text{mm (from the geometry of node } N_{13})$$

Widths of other struts are determined by developing a realistic geometry of the struts.
STM forces:

$$T_{4n,10n,max} = A_{sv} f_y = \left[\frac{\pi 10^2}{4} \times 2\text{stirrup} \times 2 - \text{legs}\right] \times 538.80 = 169.27\,\text{kN}$$

$$T_{6n,max} = A_{sv6} f_y = \left[\frac{\pi 8^2}{4} \times 2\text{stirrup} \times 2 - \text{legs}\right] \times 321.80 = 64.70\,\text{kN}$$

$$T_{7n,max} = A_{sh7} f_y = \left[\frac{\pi 13^2}{4} \times 2\right] \times 513.60 = 136.34\,\text{kN}$$

$$T_{11n\text{ to }14n,1n,max} = A_{sh} f_y = \left[\frac{\pi 13^2}{4} \times 4\right] \times 513.60 + \left[\frac{\pi 10^2}{4} \times 4\right] \times 538.8 = 442\,\text{kN}$$

$$T_{2n,9n,max} = A_{sv} f_y = \left[\frac{\pi 6^2}{4} \times 2\text{stirrup} \times 2\text{legs}\right] \times 355.20 = 40.17\,\text{kN}$$

The reinforcement details are shown in Fig. 2b. The struts, ties, and nodes are labeled as in Fig. 2d–f, respectively. The forces in all members (calculated form static) are as in Table 11.

Checking of stress limits:

(a) Concrete Struts: Knowing that $f'_c = 36.20$ MPa, the term $\left(f_{ce} = 0.85 f'_c \beta\right)$ will be:

Table 12 Concrete strut calculations of beam IT1, Fig. 2

Model label	f_{ce}^{sj} (MPa)	Strut width (mm)	Max. strut capacity (kN)	Actual strut force (kN)	Status
1	24.62	140.88	693.69	154.95	Yes
2	24.62	57.00	280.67	168.10	Yes
3	24.62	43.00	211.73	111.50	Yes
4	24.62	57.00	280.67	161.91	Yes
5	30.77	43.00	264.62	113.60	Yes
6	30.77	44.31	272.68	100.92	Yes
7	24.62	57.00	280.67	162.44	Yes
8	30.77	43.00	264.62	1.43	Yes
9	30.77	44.31	272.68	213.10	Yes
10	24.62	57.00	280.67	29.1	Yes
11	30.77	44.31	272.68	303.29	No
12	24.62	95.00	467.78	161.93	Yes
13	24.62	57.00	280.67	163.00	Yes

Yes = Safe strut capacity and No = Unsafe strut capacity

Table 13 Calculations of critical concrete nodes of beam IT1, Fig. 2

Model label	Type	βn	Surrounding forces (kN)	C or T	Available width (mm)	f_{ce}^{ni} (MPa)	Max. capacity (kN)	Actual force (kN)	Status
11	CCT	0.80	154.95	C	140.88	24.62	693.69	154.95	Yes
		0.80	101.02	T	100.00	24.62	492.40	101.02	Yes
		0.80	117.50	C	100.00	24.62	492.40	117.50	Yes
3	CCT	0.80	154.95	C	140.88	24.62	693.69	154.95	Yes
		0.80	111.50	C	43.00	24.62	211.73	111.50	Yes
		0.80	124.00	T	55.00	24.62	270.82	124.00	Yes
		0.80	12.34	T	45.00	24.62	221.58	12.34	Yes
13	CCC	1.00	303.29	C	44.31	30.77	272.68	303.29	No
		1.00	161.93	C	95.00	30.77	584.63	161.93	Yes
		1.00	235.00	C	200.0	30.77	1230.8	235.00	Yes

$$f_{ce}^{sj} = 0.85 f_c' \beta_{sj} = 0.85 \times 36.20 \times 1.00 = 30.77\,\text{MPa}, \text{ for Strut Sj } (j = 5, 6, 8, 9, \text{ and } 11)$$

$$f_{ce}^{sj} = 0.85 f_c' \beta_{sj} = 0.85 \times 36.20 \times 0.80 = 24.62\,\text{MPa}, \text{ for Strut Sj } (j = 1 \text{ to } 4 \text{ and } 7,\ 10,\ 12, \text{ and } 13)$$

Maximum strut capacity, $S_{jn,max} = f_{ce}^{sj} b w_j$. All struts' calculations are given in Table 12.

(b) Nodes:

Maximum node capacity is $f_{ce}^{ni} b w_i$ where $f_{ce}^{ni} = 0.85 f_c' \beta_{ni}$, Table 13. The *nominal shear force* is:

$$V_n = 117.5\,\text{kN},\ P_{STM} = 2V_n = 235\,\text{kN} \times \frac{272.68}{303.29} = 211.28\,\text{kN}, \text{ and } P_{STM}/P_{EXP} = \frac{211.28}{314.67} \cong 0.70$$

Appendix C: Numerical Scheme of Beam DSON3, Fig. 4

Input data:

$f_c' = 30.45$ MPa, $f_y = 410$ MPa for 16 mm bars, $f_{yv} = 244.5$ MPa for 6 mm bars, $f_{yh} = 260.2$ MPa for 8 mm bars, A_s' (4–10 mm bars), and A_s (4–16 mm bars) = 804.25 mm^2, Fig. 4b. To simplify visualization of strut widths and geometry of nodes, the simplified STM in Fig. 4d is used.

Width of struts:

The strut widths were determined by developing a realistic geometry of the struts as they extend from the nodes, Fig. 4e. The term a_1 (height of node N_1) is:

$$a_1 = n\emptyset_{bars} + 2c + (n-1)\,s = 2 \times 16 + 2 \times 24 + (2-1) \times 0 = 80\,\text{mm}.$$

Table 14 STM calculated forces of beam DSON3 [10]

Model label	Force (kN)	C or T	Model label	Force (kN)	C or T
S1	64.14	C	T1	61.59	T
S2	58.04	C	T2	4.27	T
S3	75.42	C	T3	46.86	T
S4	48.44	C	T4	37.04	T
S5	31.34	C	T5	22.46	T

STM forces: The forces in all members are determined from statics, and their magnitudes are as indicated in Table 14. The struts, ties, and nodes are labeled as in Fig. 4d.
$T_{1n,max} = A_s f_y = 804.25 \times 410 = 329.74\,\text{kN}$ where $T_{in,max}$ is the nominal strength capacity of the tie i when reaching its yield strength. Finally, $P_{STM} = 2V_n = 2 \times 64 = 128\,\text{kN}$

Checking of stress limits:

a. Concrete Struts: Knowing that $f'_c = 30.45\,\text{MPa}$, the term $\left(f_{ce} = 0.85 f'_c \beta\right)$ will be:

$$f_{ce}^{sj} = 0.85 f'_c \beta_{sj} = 0.85 \times 30.45 \times 1.00 = 25.88\,\text{MPa}, \text{ for Strut } S_j\ (j = 2, 5)$$
$$f_{ce}^{sj} = 0.85 f'_c \beta_{sj} = 0.85 \times 30.45 \times 0.80 = 20.71\,\text{MPa}, \text{ for Strut } S_j\ (j = 1, 3, \text{ and } 4)$$

Table 17 STM forces of proposed simplified STM of beam DSON3 [10]

Model label	Force (kN)	T or C	Model label	Force (kN)	T or C
S1	66.29	C	T1	72.39	T
S2	75.25	C	T2	13.00	T
S3	91.81	C	T3	27.00	T
S4	88.11	C	T4	17.33	T
S5	37.58	C	T5	53.27	T
S6	43.00	C	T6	6.47	T
S7	65.27	C	T7	6.47	T
S8	12.83	C	–	–	–

Maximum strut capacity is given by $S_{jn,max} = f_{ce}^{sj} b w_j$. All struts data are shown in Table 15.
(b) Nodes:

Table 16 summarizes the calculations performed for the critical nodes N_1, N_3, and N_4. The maximum node capacity is given by $f_{ce}^{ni} b w_i$ where $f_{ce}^{ni} = 0.85 f'_c \beta_{ni}$. The safe solution yields:

$$P_{STM} = 128\,\text{kN} \times \frac{71.24}{75.42} = 121.0\,\text{kN} \quad \text{and}$$
$$P_{STM}/P_{EXP} = \frac{121.00}{140.00} = 0.86$$

Table 15 Concrete strut calculations of beam DSON3 [10]

Model label	β s	f_{ce}^{sj} MPa	Strut width	Max. strut capacity (kN)	Actual Strut force (kN)	Status
1	0.80	20.71	52.00	86.15	64.14	Yes
2	1.00	25.88	53.00	109.73	58.04	Yes
3	0.80	20.71	43.00	71.24	75.42	No
4	0.80	20.71	42.00	69.59	48.44	Yes
5	1.00	25.88	52.00	107.66	31.34	Yes

Table 16 Calculations of critical concrete nodes of beam DSON3 [10]

Model label	Type	βn	Surrounding forces (kN)	C or T	Available width (mm)	f_{ce}^{ni} (MPa)	Max. capacity (kN)	Actual force (kN)	Status
1	CCT	0.80	64.14	C	94.00	20.71	155.71	64.14	Yes
		0.80	64.00	C	100.00	20.71	165.68	64.00	Yes
		0.80	4.27	T	80.00	20.71	132.54	4.27	Yes
4	CCC	1.00	75.42	C	43.00	25.88	89.03	75.42	Yes
		1.00	48.44	C	42.00	25.88	86.96	48.44	Yes
		1.00	128.0	C	100.0	25.88	207.04	128.0	Yes
3	CTT	0.60	31.34	C	52.00	15.53	63.77	31.34	Yes
		0.60	46.86	T	55.00	15.53	68.33	46.86	Yes
		0.60	4.27	T	69.00	15.53	85.73	4.27	Yes
		0.60	61.59	T	69.00	15.53	85.73	61.59	Yes

Table 18 Concrete strut calculations of the simplified STM using vertical and horizontal ties of beam DSON3 [10]

Model label	βs	f_{ce}^{sj} MPa	Strut width (mm)	Max. strut capacity (kN)	Actual strut force (kN)	Status
1	1.00	25.88	113.0	233.96	66.29	Yes
2	1.00	25.88	62.00	128.36	75.25	Yes
3	1.00	25.88	59.00	122.15	91.81	Yes
4	1.00	25.88	52.00	107.66	88.11	Yes
5	1.00	25.88	36.00	74.53	37.58	Yes
6	1.00	25.88	47.00	97.31	43.00	Yes
7	1.00	25.88	51.00	105.59	65.27	Yes
8	1.00	25.88	62.00	128.36	12.83	Yes

Table 19 Calculations of critical concrete nodes of the simplified STM using vertical and horizontal ties of beam DSON3 [10]

Model label	Type	βn	Surrounding forces (kN)	C or T	Available width (mm)	f_{ce}^{ni} (MPa)	Max. capacity (kN)	Actual force (kN)	Status
1	CCT	0.80	65.00	C	100.00	20.71	165.70	65.00	Yes
		0.80	66.29	C	113.0	20.71	187.22	66.29	Yes
		0.80	13.00	T	80.00	20.71	132.54	13.00	Yes
5	CCC	1.00	130.0	C	100.0	25.88	207.04	130.0	Yes
		1.00	88.11	C	52.00	25.88	107.66	88.11	Yes
		1.00	37.58	C	36.00	25.88	74.53	37.58	Yes
8	CCT	0.80	43.00	C	47.00	20.71	77.87	43.00	Yes
		0.80	12.83	C	62.00	20.71	102.72	12.83	Yes
		0.80	65.27	C	51.00	20.71	84.50	65.27	Yes
		0.80	24.92	T	51.00	20.71	84.50	24.92	Yes
		0.80	10.13	T	63.00	20.71	104.40	10.13	Yes

The alternative proposed refined and simplified STMs for beam DSON3 using vertical and horizontal ties are shown in Fig. 4f, g, respectively. The STM forces are shown in Table 17. Finally, for the model in Fig. 4g, $P_{STM} = 2V_n = 2 \times 65 = 130\,\text{kN}$, $P_{STM}/P_{EXP} = \frac{130.00}{140.00} = 0.93$

Checking of stress limits:

(a) Concrete Struts: Knowing that $f'_c = 30.45\,\text{MPa}$, the term $\left(f_{ce} = 0.85 f'_c \beta\right)$ will be:

$f_{ce}^{sj} = 0.85 f'_c \beta_{sj} = 0.85 \times 30.45 \times 1.00 = 25.88\,\text{MPa}$, for all Struts S_j (j = 1–8), Table 18.

(b) Nodes:

Table 19 summarizes the calculations performed for the critical nodes N_1, N_5, and N_8. The maximum node capacity is $f_{ce}^{ni} b w_i$ where $f_{ce}^{ni} = 0.85 f'_c \beta_{ni}$. The safe solution of the model in Fig. 4g gives $P_{STM} = 130\,\text{kN}$; thus, $P_{STM}/P_{EXP} = \frac{130.00}{140.00} = 0.93$.

References

1. American Concrete Institute: Building Code Requirements for RC. Detroit, ACI-318M (2011)
2. El-Zoughiby, M.E.; El-Metwally, S.E.; El-Shora, A.T.; Agieb, E.E.: Strength prediction of simply supported R/C deep beams using the strut-and-tie method. Arab. J. Sci. Eng. **38**(8), 1973–1991 (2013)
3. El-Zoughiby, M.E.; El-Metwally, S.E.; El-Shora, A.T.; Agieb, E.E.: Strength prediction of continuous R/C deep beams using the strut-and-tie method. Arab. J. Sci. Eng. **39**(3), 1685–1699 (2014)
4. ANSYS-12 Package, 2009 SAS IP, Inc.
5. Egyptian Code for the Design and Construction of Reinforced Concrete Structure, Cairo, 2007, Ministry of Housing and Development of New Communities, Cairo, Egypt
6. Schlaich, J.; Schäfer, K.: Design and detailing of structural concrete using strut-and-tie models. Struct. Eng. **69**(6), 113–125 (1991)
7. Amiri, J.V.; Hosseinalibygie, M.: Effect of small circular openings on the shear and flexural behavior and ultimate strength of RC beams using normal- and high-strength concrete. In: 13th World Conference on Earthquake Engineering, Vancouver, BC, Canada (2004)
8. Abdalla, H.A.; Torkeya, A.M.; Haggagb, H.A.; Abu-Amira, A.F.: Design against cracking at openings in RC beams strengthened with composite sheets. Compos. Struct. **60**, 197–204 (2003)

9. Tan, K.H.; Mansur, M.A.; Huang, L.M.: RC T-beams with large Web openings in positive and negative moment regions. Exp. Study ACI Struct. J. **93**(3) (1996)
10. El-Azab, M.F.: Behavior of Reinforced HSC Deep Beams with Web Openings. M.Sc. Thesis, Structural Engineering, Faculty of Engineering, El-Mansoura University, El-Mansoura, Egypt (2007)
11. Mohammad, K.I.: Prediction of Behavior of Reinforced Concrete Deep Beams with Web Openings Using Finite Elements, vol. 15, No. 4. Al-Rafidain Engineering, Iraq (2007)
12. Thompson, M.K.; Young, M.J.; Jirsa, J.O.; Breen, J.E.; Klingner, R.E.: Anchorage of Headed Reinforcement in CCT Nodes. Research Report 1855-2, Austin, TX, Center for Transportation Research, University of Texas at Austin (2003)